\$ SUPER

Contents lists available at ScienceDirect

International Journal of Applied Earth Observation and Geoinformation

journal homepage: www.elsevier.com/locate/jag



Assessment and validation of Meteosat SEVIRI fire radiative power (FRP) retrievals over Kruger National Park

Gareth Roberts a,*, Martin. J. Wooster b, Tercia Strydom c

- ^a School of Geography and Environmental Science, University of Southampton, Southampton, UK
- b NERC National Centre for Earth Observation (NCEO) and the Leverhulme Centre for Wildfires, Environment and Society, c/o Department of Geography, Kings College London. WC2R 2LS. UK
- ^c Scientific Services, South African National Parks, Skukuza, South Africa

ABSTRACT

Satellite burned area, active fire and fire radiative power (FRP), are key to quantifying fire activity and are one of 54 essential climate variables (ECV) and it is important to validate these data to ensure their consistency. This study investigates some of the factors that influence FRP retrieval and uses Meteosat Spinning Enhanced Visible and InfraRed Imager (SEVIRI) data to do so. Analysis of the influence of a fire's location within a SEVIRI pixel on FRP was carried out using fire simulations which indicate that FRP varies by up to 14 % at nadir for a single sensor and by up to 55 % when intercomparing simulated FRP from different SEVIRI sensors. Intercomparison between actual MET-11 and MET-08 FRP data on a per-pixel basis reveals a high degree of scatter (81.9 MW), strong correlation (R = 0.72), low bias (\sim 1 MW) and an average percentage difference of 15.7 %. Variability is reduced when aggregated to fire 'clusters' which improves the correlation (R = 0.96) and reduces the average percentage difference (4.2 %). Validation of MET-08 and MET-11 FRP retrievals using FRP from helicopter mounted longwave infrared (LWIR) thermal cameras is carried out over five prescribed burns. The results reveal good agreement between the SEVIRI and thermal camera FRP although the SEVIRI FRP is typically overestimated compared to that from the LWIR camera. This study illustrates some of the challenges validating satellite FRP which should be accounted for when defining uncertainty thresholds for product requirements and in developing FRP validation protocols.

1. Introduction

Landscape fires burn across an average of 4.6 million km² of the Earth surface annually (Lizundia-Loiola et al., 2020), altering the surface radiative and structural properties by consuming vegetation and organic soils and releasing large quantities of smoke into the atmosphere (Jin et al., 2012; van der Werf et al., 2017). The latter contains fine particulate matter (PM2.5), which impacts air quality leading to hundreds of thousands of premature deaths annually in people exposed to smoke polluted air (Roberts and Wooster, 2021; Xue et al., 2021). To quantify landscape fire emissions, satellite Earth Observation focused on burned area mapping or the detection of radiant heat from fires is pivotal. Here we focus on the latter, which uses algorithms to identify pixels containing an active fire (AF) by exploiting the differential sensitivity of LWIR (8 – 14 μ m) and MWIR (3 – 5 μ m) spectral bands to high temperature sub-pixel phenomena. Once detected each AF pixel has its FRP quantified using the MWIR spectral radiance anomaly over the surrounding non-fire background (Wooster et al., 2021). Satellite 'thermal anomalies products' have been developed for polar-orbiting (e.g. Giglio et al., 2016; Wooster et al., 2012; Schroeder et al., 2014a). and geostationary sensors (Schmidt et al., 2012; Wooster et al., 2015; Xu et al.,

2017).

Along with burned area, satellite AF and FRP data represent ECVs as designated by the Global Climate Observing System (GCOS). Given this it is imperative that satellite AF products are evaluated for their performance and accuracy, and guidelines for doing this are being developed by the Land Product Validation (LPV) subgroup of the Committee Earth Observing Satellites' Working Group on Calibration and Validation (CEOS WGCV; Morisette et al., 2006). The current validation stage of satellite burned area and AF information, which defines the comprehensiveness of the methods used to assess the products spatial and temporal information, is stage three (Boschetti et al., 2019; Giglio et al., 2016). However, FRP is currently at validation stage one, indicating product accuracy has been assessed over a limited number of locations and time periods. This is in part because of difficulties collecting suitable reference measurements since fires occur over large diurnal and seasonal activity cycles (Roberts et al., 2009; Giglio et al. 2006) and can exhibit rapid changes in their FRP. This poses a problem for the collection of reference data which needs to be obtained contemporaneously to the data to which it is compared and be unsaturated to provide accurate FRP. Beyond these characteristics, there are other factors influencing satellite AF evaluation that are not commonly

E-mail addresses: G.J.Roberts@soton.ac.uk (G. Roberts), martin.wooster@kcl.ac.uk (Martin.J. Wooster), tercia.strydom@sanparks.org (T. Strydom).

^{*} Corresponding author.

considered in validation efforts. Here we start to explore these issues, demonstrating them using both simulated and real FRP retrievals, the latter made using Meteosat SEVIRI data of fires burning in Kruger National Park (KNP, South Africa).

Firstly, using the SEVIRI point spread function (PSF) and simulated active fire observations, we conduct a simulation study illustrating the impact that a fire's sub-pixel location has on its FRP retrieval. We then highlight some of the challenges of intercomparing and evaluating FRP retrievals made from even the same sensor but using different viewing geometries, by intercomparing FRP data of the same fires made by the standard Meteosat (located at on the equator over West Africa), and Meteosat Indian Ocean (IODC; located over East Africa). Using 456 experimental fires conducted in the KNP, the influence of pixel area on the detection of actively burning fires is assessed. Finally, the accuracy of the satellite FRP retrievals made over five experimental fires is assessed using simultaneous airborne thermal infrared measurements made in both LWIR and MWIR wavebands, helping demonstrate which reference data source is more appropriate and whether the satellite-toairborne differences identified are within the range suggested by the aforementioned simulations.

1.1. Background to active fire (AF) product evaluation

Evaluation of moderate spatial resolution AF detection data commonly involves intercomparison to contemporaneous higher spatial resolution AF data derived using shortwave infrared (SWIR; 1.6 and 2.2 μm) observations which are sensitive to thermal emissions from high temperature targets even by day when a significant solar radiation signal is present (e.g. Giglio et al., 2016; Hall et al., 2019; Schroeder et al., 2010). This enables AF detection errors of omission and commission to be determined for a given region, potentially for different seasons and times of day. Studies have exploited the availability of a high (Advanced Spaceborne Thermal Emission and Reflection Radiometer, ASTER) and moderate (Moderate Resolution Imaging Spectroradiometer, MODIS) spatial resolution sensors onboard the Terra platform (Schroeder et al., 2008; Giglio et al., 2016). This approach allowed global validation of the AF detections from the Terra MODIS AF product, though only in the centre of the MODIS swath. More generally, such intercomparisons rely on data from sensors on different platforms, and this usually involves allowing a temporal offset (e.g. 2-10 min) between the datasets to ensure a sufficiently large sample (Xu et al., 2020; Wickramasinghe et al., 2018).

Validating satellite FRP retrievals is more challenging still, with the high rate of change of FRP requiring a minimal time difference between datasets (Freeborn et al., 2014). Such comparisons are generally carried out at the 'fire cluster' or grid cell scale, due to the different pixel sizes of the AF datasets (e.g. Xu et al., 2010; Vermote et al., 2009). Other potential difficulties relate to the influence of sub-pixel cloud and smoke, viewing geometry, the fire's location within the IFOV, and the presence of overlying vegetation (Roberts et al., 2018; Kumar et al., 2020; Calle et al., 2009; Schroeder et al., 2010; Freeborn et al., 2011). The CEOS LPV stage of FRP validation is stage one and most efforts have focused on satellite product intercomparisons (Xu et al., 2021; Zhukov et al., 2006). Most validation attempts have used of prescribed burns, with reference data being collected with handheld, tower or aircraft mounted thermal infrared imagers. The largest effort so far has been the RxCADRE experiment (2012), where temporally coincident MODIS and VIIRS FRP retrievals were compared to airborne Wildfire Airborne Sensor Program (WASP) data (Dickinson et al., 2016). The satellite FRP was generally lower than the airborne FRP and attributed to the influence of cloud and to potential LWIR airborne imager calibration issues. Schroeder et al. (2014b) compared MODIS and Geostationary Operational Environmental Satellite (GOES) FRP retrievals with those from NASAs Autonomous Modular Sensor-Wildfire (AMS), also finding widely varying differences of 5 to 110 %.

2. Datasets

2.1. Meteosat FRP products

This study focuses on the evaluation of FRP retrievals from AF pixels detected in data captured by the SEVIRI onboard the Meteosat Second Generation (MSG). This geostationary satellite system has operated since the MET-08 launch in 2002, and MET-09, -10 and -11 launches in 2005, 2012 and 2015 respectively. The nominal location for the MSG satellites is 0° latitude, 0° longitude, and in 2017 MET-08 was repositioned to 41.5 $^{\circ}$ E, 0° North to provide an IODC (Fig. 1). For simplicity, we hereafter refer to MET-08 when describing SEVIRI acquisitions obtained from the IODC coverage position and MET-11 to describe any obtained from the nominal 0° N, 0° E position.

SEVIRI observes in 11 spectral channels and at a temporal resolution of 15 min. Except for the broadband visible channel, each spectral channel is measured with a point spread function (PSF) that provides an IFOV of 4.8 km, sampled at an interval of 3 km and an oversampling factor of 1.6 (Schmetz et al., 2002). The Meteosat Active Fire Detection and FRP products (Wooster et al., 2015) are produced from geocoded and radiometrically calibrated level 1.5 data by the Land Surface Analysis Satellite Applications Facility (LSA-SAF, Trigo et al., 2011), with the FRP-PIXEL product generated at SEVIRI's native spatiotemporal resolution. Intercomparisons conducted between the FRP-PIXEL product and those of MODIS indicate that when both detect the same fire within \pm 6 mins there is a strong agreement and low bias in their FRP retrievals (e.g. Roberts et al., 2015; Roberts and Wooster, 2008). However, when imaging a region, SEVIRI underestimates FRP with respect to MODIS due to it being unable to detect low FRP AF pixels due to its larger pixel area. For the MET-11 FRP-PIXEL product this results in AF detection errors of omission of 65 % in Northern Hemisphere Africa and 77 % in Southern Hemisphere Africa where the pixel area is larger (Roberts et al., 2015). Hall et al. (2019) intercompared the FRP-PIXEL and other geostationary satellite AF products to nearsimultaneous AF detections made using Landsat Operational Land Imager (OLI), which has 30 m pixels. The results indicate variations in geostationary AF pixel detection rate are a function of the fractional area actively burning and that ~75 – 80 % of AF pixels are detected when at least 2 % of the pixel was burning.

3. Study location and reference data

3.1. Kruger National Park (KNP)

The region selected for FRP product assessment is the KNP, a protected area covering 19,500 km². This is viewed by MET-11 at a mean view zenith angle (VZA) of 45° and by MET-8 at 30° and is subject to frequent wildfires between August and October, as well as hosting a long-standing experimental burn programme (Biggs et al., 2003). This programme was initiated in 1954 to understand the role of fire frequency and seasonality on herbaceous and woody savannah vegetation structure. Experimental burn plots (EBPs) are located in 16 burn site 'replicates', with four in each of the parks four veld landscapes, and each hosting a string of 12 EBPs with mean area of 7 ha (Fig. 2). EBPs in each replicate string are subjected to fire 'treatments', differing by seasonality (February, April, August, October, or December ignition) and frequency (burned every 1, 2, 3, 4 or 6 years). Most EBPs are subject to annual, biannual, or tri-annual burns, with some plots excluded from burning entirely but subject to other disturbances such as herbivory. EBPs highlighted by blue symbols in Fig. 2 are the sites of airborne data collection used to create the reference data for evaluating SEVIRI FRP retrievals.

3.2. Airborne thermal imagery

The reference fires had their FRP measured using helicopter-

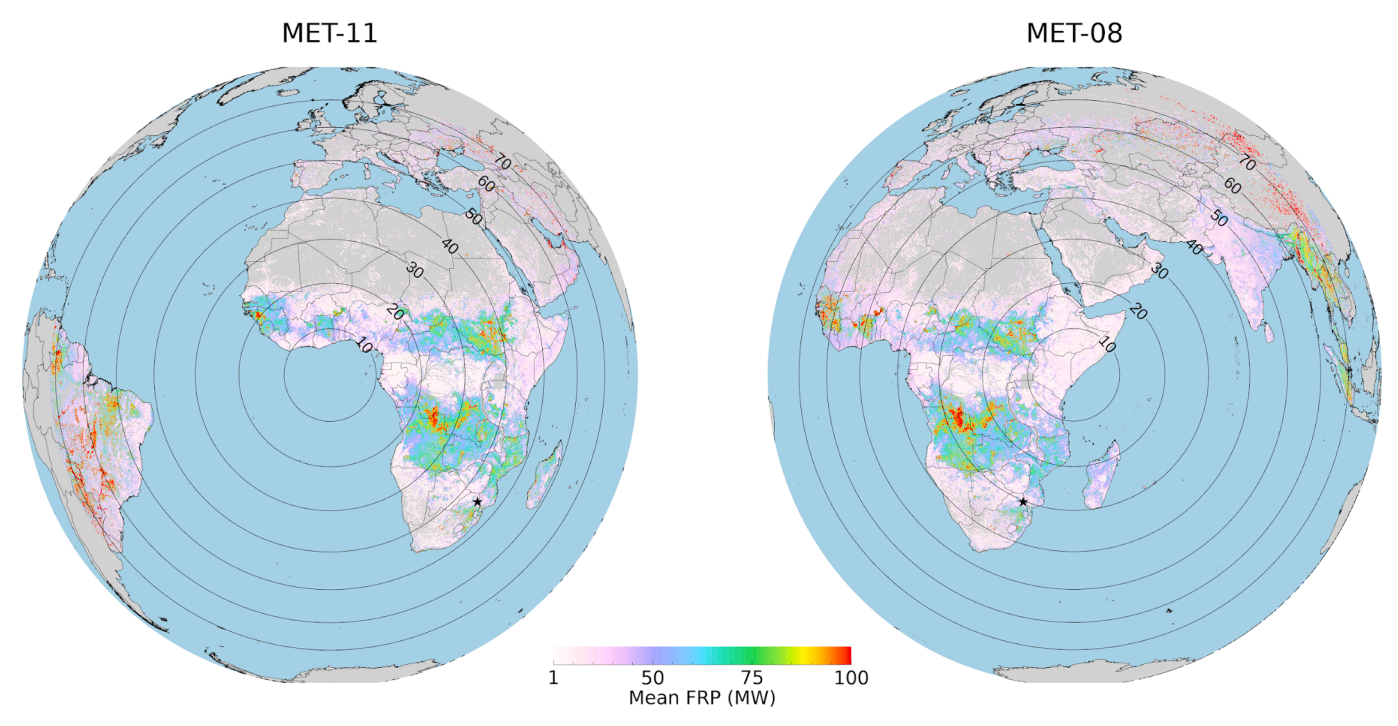


Fig. 1. Mean (2017–2020) per-pixel FRP (MW) derived from the MET-11 and MET-08 IODC FRP-PIXEL products. Overlain are the SEVIRI view zenith angles (10 – 70°) with the KNP marked by black star.

mounted MWIR and LWIR cameras fitted with a 3.9 μm and 10.8 μm narrowband filter respectively. The MWIR camera was an AGEMA 550 InSb cooled detector system offering 30 Hz data covering 320 x 240 pixels across a 40° FOV. This camera measures brightness temperatures (BT) in the range -20 and 1500 °C but separated into three intervals – of which the 250 – 700 °C range was used to prevent pixel saturation. The LWIR camera was an Infratec VarioCAM HD 600, an uncooled microbolometer system set to record at 30 Hz but across a wider 640 x 480 array and a 30 x 23° FOV. We used a 0 – 850 °C BT measurement range for this camera.

Both cameras were deployed from a helicopter flown ~ 600 m above the EBP fires which ensured that the entire EBP fell within the cameras FOV. Assuming a 45° view zenith angle to the plot centre, the pixel sizes of the AGEMA and VarioCAM HD cameras are ~ 2.6 m $\times 3.4$ m (9.1 m²) and 1.05 \times 1.05 m (1.1 m²) respectively, though this varied over time and between different fire acquisitions. To aid imagery geo-location and the pixel area derivation necessary for FRP retrieval, fires were lit at each EBP corner to act as ground control points (GCPs). Improving on the manual georectification applied here, Paugam et al. (2012; Paugam et al, 2021) developed a method for automatically aligning thermal camera imagery.

4. FRP uncertainty Investigations

4.1. Sensitivity to fire Sub-Pixel location

We first analysed the FRP products sensitivity to the fire's sub-pixel location within the IFOV which influences the sensors response to the fire emitted MWIR spectral radiance (Calle et al., 2009; Freeborn et al., 2014; Xu et al., 2021). We conducted a series of simulations where we moved a uniform sub-pixel sized fire around within a pixel to examine the effect on FRP retrieval. The fire had a homogeneous temperature and fixed size and was located at different positions within the simulated SEVIRI pixel, which have a rhombus shaped PSF (Coppo, 2015). Fires were simulated using 100 m grid cells and at temperatures of 500, 800 or 1000 K and were positioned over the mean size of an EBP (300 x 200 m).

The simulated image covered 51 \times 51 km, giving sufficient non-fire

background which had a 300 K temperature. Simulations were conducted with the fire shifted up to 2500 m either side of the PSF centre in 100 m increments in the along-scan direction. SEVIRI 3.9 µm spectral radiances were convolved with the PSF to generate simulated SEVIRI observations, which were then convolved with the finite impulse response (FIR) filter (Wooster et al., 2015). The latter is a 17-pixel wide symmetric Sinc function kernel, applied to the Level 1.0 data to generate Level 1.5 data (Schmetz et al., 2002). The simulated SEVIRI data were converted into BT (K) and 'fire affected pixels' then identified using a 2.5 K BT difference above background, a threshold like that used to generate the FRP-PIXEL product. Analysis of FRP-PIXEL product data (2014—2019) indicates the mean fire pixel MWIR BT elevation above the background is 6.7 K (median of 5.3 K), so a 2.5 K difference will detect some of the lowest FRP fire pixels SEVIRI can identify.

Our simulations confirm the findings of Freeborn et al. (2014) for MODIS, that real FRP retrievals always have an uncertainty component stemming from our imprecise knowledge of the fires sub-pixel location. This source of uncertainty is not yet built into the uncertainty metric present in some FRP products – including the FRP-PIXEL product. Based on multiple simulations, each with different sub-pixel fire locations and/or temperatures, Fig. 5 shows the numbers of AF pixels detected, total pixels saturated (> 335.5 K), and retrieved FRP. Fig. S1 shows the impact of a fire's sub-pixel location on the BT of the simulated AF pixels, and their along-scan neighbours.

The distribution of retrieved FRP with distance from the PSF centre is influenced by the number of AF pixel detections and the number of saturated pixels. The sensitivity of the FRP profile to the fires sub-pixel location demonstrates the impact of the FIR filter, which serves to increase and decrease the PSF weighting in the along-scan direction. The nature of this variation depends on the fire's specific characteristics. When the fire is at or close to the PSF centre the FRP is relatively well retrieved due to a combination of the fire size, degree of saturation and the effect of the FIR filter sidelobes which reduce the BT of the pixels neighbouring the AF pixels — thus increasing the latter's BT elevation above the background (Fig. S1). For a 500 K fire, the abrupt FRP profile is due to the variation in the number of detected fire pixels caused by the low pixel BTs and the comparatively large (at these temperatures) BT

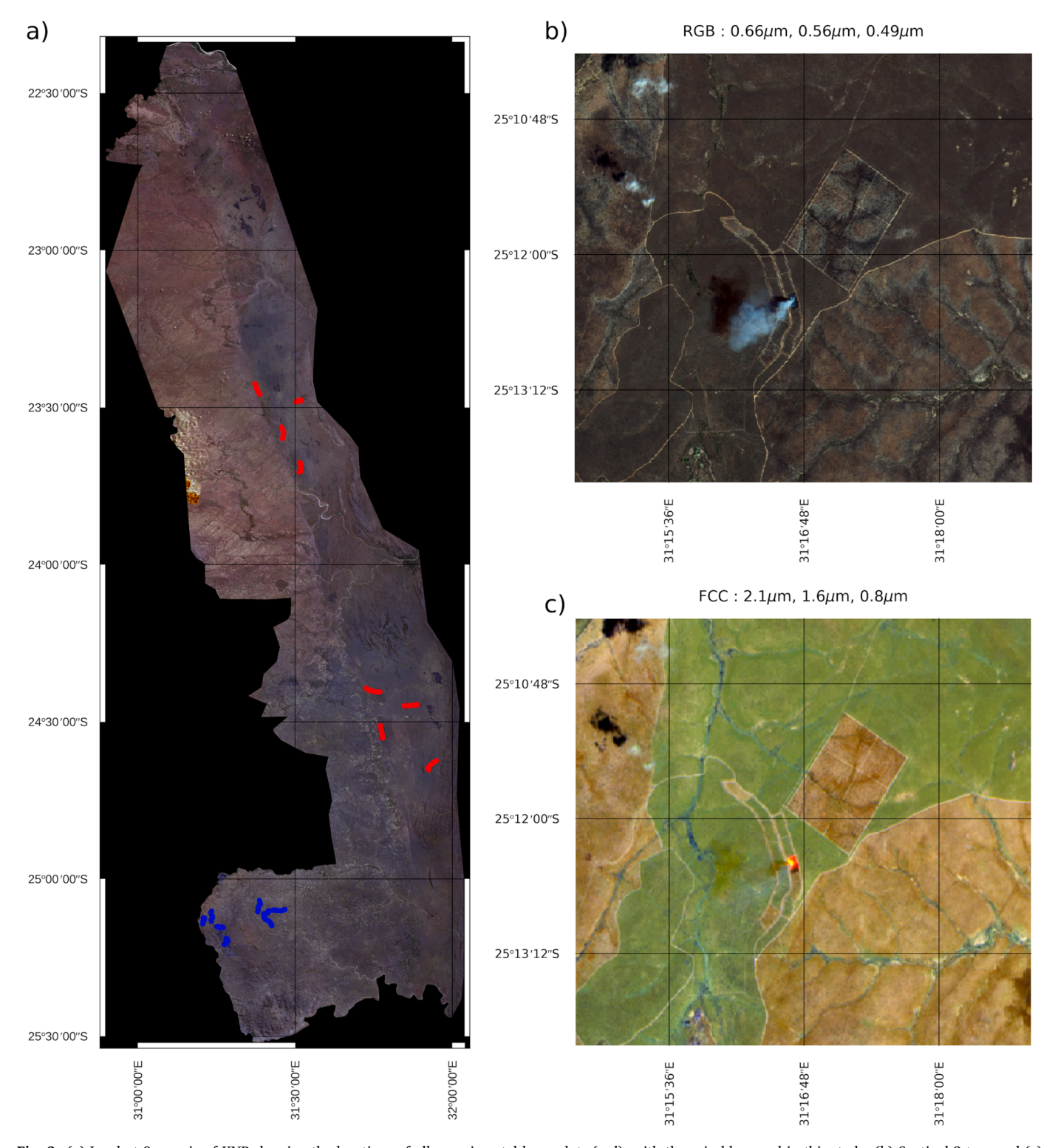


Fig. 2. (a) Landsat 8 mosaic of KNP showing the locations of all experimental burn plots (red), with those in blue used in this study. (b) Sentinel-2 true and (c) infrared false colour images which captured an EBP fire on 16th October 2018.

difference required to identify an AF pixel. The influence of the FIR filter is more apparent at higher fire temperatures, with depressed background BTs at distances of two and four pixels from the pixel centre. When the fire is centrally located within a pixel, the FRP is constrained by a combination of fewer detected AF pixels, and, at higher fire temperatures, pixel saturation which affects 9 and 22 % of the fire pixels at 800 and 1000 K respectively. When located away from the pixel centre, the FRP differs by up to 12, 14 and 11 % with respect to when the fire is

centrally located for 500, 800 and 1000 K fires respectively. The influence of image filtering on fire detection is illustrated in Fig. S2 which shows, for each fire temperature, the simulated nadir SEVIRI BT, the retrieved FRP, and the location of detected fire and saturated pixels. Also shown are actual SEVIRI MWIR image subsets that display similar spatial patterns of BT as the simulations although the temperature and size of these fires is unknown.

Simulations for MET-08 and MET-11 that focused on the viewing

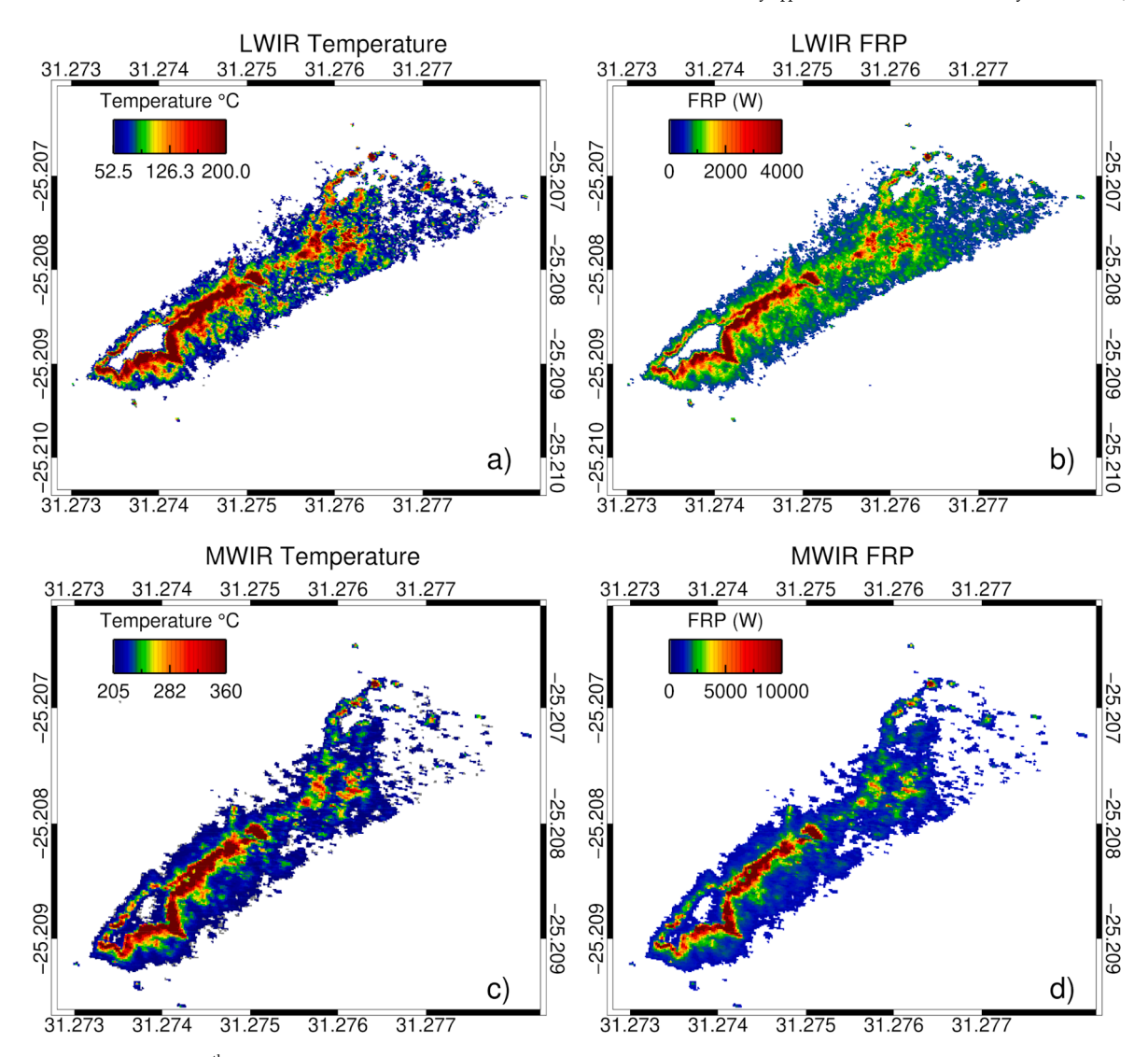


Fig. 3. KNP experimental burn (27th August 2019) observed by helicopter borne infrared cameras. a) LWIR BT (°C) and b) per-pixel FRP (W), and c) co-incident MWIR BT (°C) and d) FRP (W).

geometries found over KNP were generated using the same $3 \times 2\,100\,\text{m}^2$ fire pixels and fire temperatures. The SEVIRI PSF for MET-08 and $-11\,$ were used, being rotated, and scaled according to the pixel dimensions found over KNP (3.1 \times 4.5 km for MET-11 and 3.1 \times 3.6 km for MET-08). Fires were positioned at intervals of 100 m radius from the PSF centre and at increments of $\sim 17^{\circ}$ in azimuth angle – resulting in 822 locations within the MET-08 and MET-11 PSF's. Fig. 6 shows the percentage difference in the FRP retrieved from the MET-11 and MET-08 simulations. For each fire temperature, the minimum difference occurs when the fire is centrally located in the MET-11 PSF, and as the fire moves away from this point the FRP difference increases to a maximum of 58 % (range -6.5 to 52 %), 20 % (14.6 to 35.5 %) and 38 % (7.7 to 46.7 %) for fire temperatures of 500, 800 and 1000 K respectively. Some of the effect is due to different numbers of fire pixels being detected for the different MET-11 and MET-08 viewing geometry data, and some to do with the differing extent of pixel saturation which can be extensive at the higher fire temperatures simulated here.

4.2. MSG-11 and MSG-8 FRP intercomparison over KNP

The simulations described in Section 4.1 illustrate the variation in retrieved FRP that may occur due to the imaging process when quantifying sub-pixel high temperature phenomenon located within a pixel. All

other perturbations were omitted (e.g. temporal offsets, spectral waveband differences, atmospheric and surface variation), and to examine these together we intercompare simultaneously acquired MET-11 and MET-08 FRP data.

Fig. 7 presents a comparison of the spatially and temporally coincident MET-11 and MET-08 FRP retrievals within KNP. Comparisons were made on a per fire pixel (Fig. 7a) and per-fire cluster (Fig. 7b) basis, using imagery acquired between 2017 and 2020. The latter refer to 'clusters' of adjacent AF pixels that can comprise of one or more pixels, each of which contain one or more active fires. On a per-pixel basis, there is good agreement with a correlation coefficient of 0.72 (R), and low bias (-1 MW). However, despite the two datasets being acquired at the same time, there is a high degree of scatter. The slope of the linear best fit is also less than unity (0.72). This variability reduces when the data are grouped into contiguous clusters of AF pixels, as is common with comparisons of AF data from different sensors (Li et al., 2018; Schroeder et al., 2010). The correlation coefficient (R) increases to 0.95, with a low bias (0.25 MW) and a linear best fit slope close to unity (0.96). The scatter also reduces, with a fire cluster mean percentage difference between MET-11 and MET-08 FRP data of 4.2 % compared to 15.7 % in the per-pixel case. As evident from Section 4.1, the fires' location within the IFOV of each sensor contributes to per-pixel FRP variability due to the fire emitted radiance being distributed into

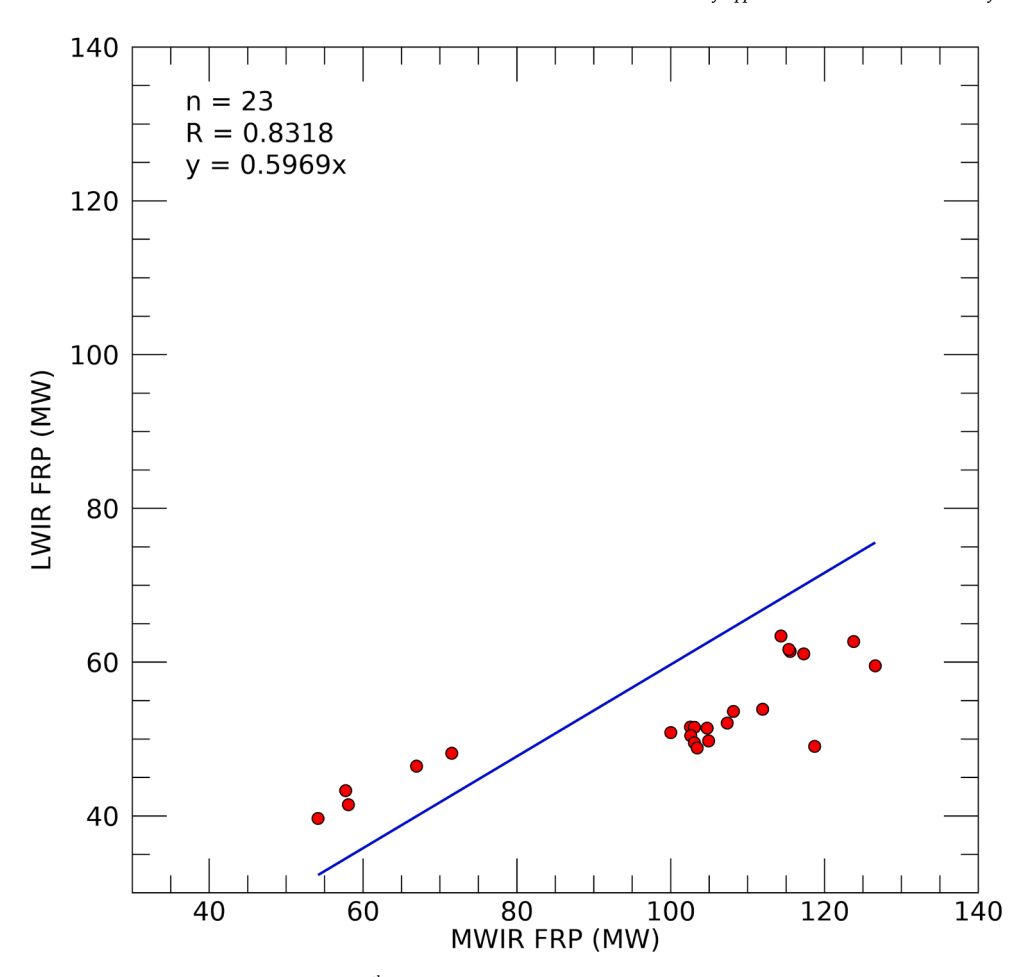


Fig. 4. FRP retrievals for a single EBP fire conducted in KNP (27th August 2019), derived from helicopter borne MWIR and LWIR imagery acquired simultaneously. Linear best fit to the data is also shown.

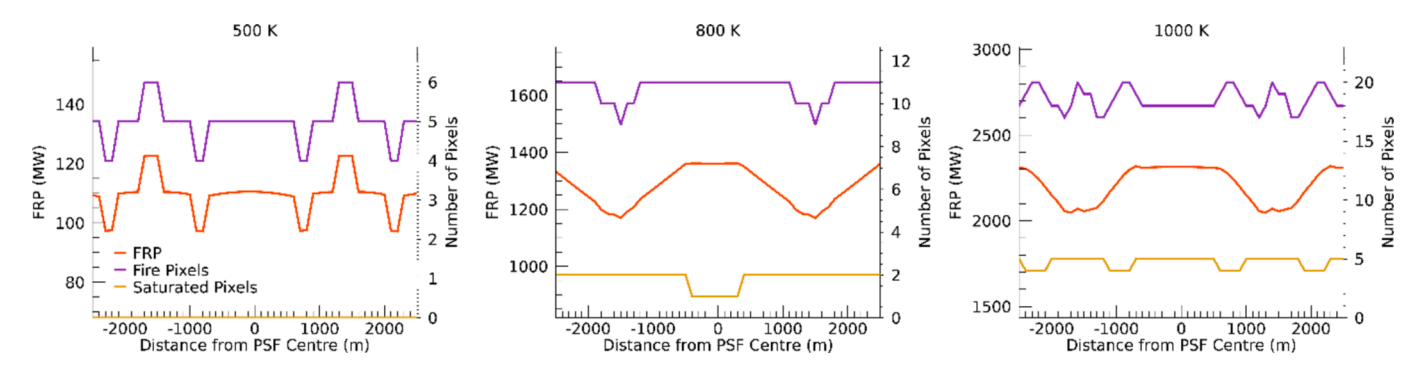


Fig. 5. Variation of image FRP and the number of fire and saturated pixels detected as a function of the fires position along an East/West transect across the image for a fire comprised of six 100 m² pixels with a uniform temperature of 500, 800 and 1000 K.

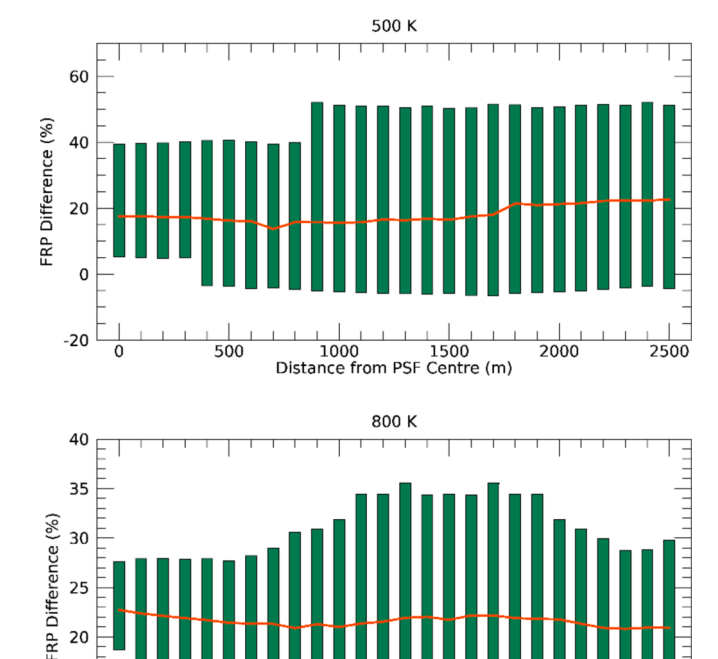
neighbouring pixels (Fig. S2). When fire pixels are spatially aggregated into clusters, the influence of the PSF is dampened as all fire emitted radiance is included in the assessment and larger clusters will be more likely to have a larger proportion of their MWIR spectral radiance located in detected AF pixels than smaller clusters or single pixel fires (Fig. 7b). This assumes that the fire emitted radiance distributed to neighbouring pixels is sufficient to elevate their BT above the background to be detected as a fire pixel.

4.3. Comparison to KNP experimental burn plots (EBP)

The detection success of the EBPs fires by Meteosat SEVIRI was used

to investigate the variation in active fire detection errors of omission between MET-11 (standard) and MET-08 (IODC). Each EBP burn has its ignition and end time recorded, and all records between 2004 and 2018 were compared to the satellite fire detections. Of the 456 EBP fires examined, only 9 (1.9 %) were detected by MET-11 and only 1 by MET-08. There was a total of 19 AF pixel detections across these 9 fires, all in the Aug or Oct burns when herbaceous fuel moisture is low and fire intensity peaks (Govender et al., 2006). These data had a per-pixel FRP ranging from 33 to 227 MW (mean of 86 MW). Burns in April and December are typically patchy, and sometimes do not result in a spreading fire making them poor targets for satellite AF detections.

Restricting our analysis to fires that occur in August and October,



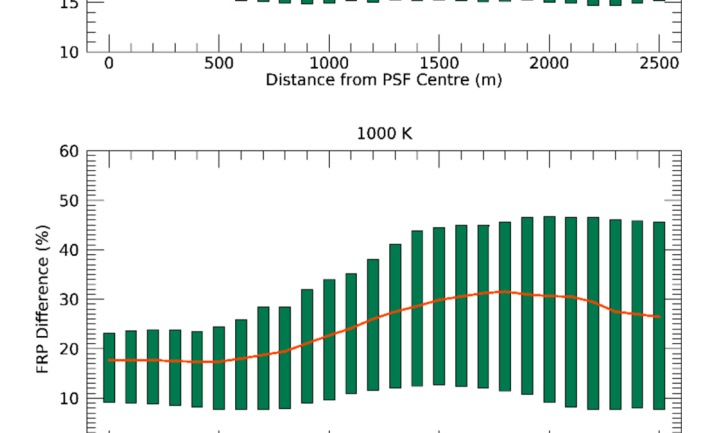


Fig. 6. Percentage difference between MET-11 and MET-08 retrieved FRP for fires simulated at 822 different locations within the MET-08 PSF at 100 m radial distances from the pixel centre. The green bars show the minimum and maximum FRP percentage difference whilst the orange line indicates the median value.

1000 1500 Distance from PSF Centre (m)

which equates to 79 % and 92 % of prescribed fires with data from MET-11 and MET-08, marginally improves the AF detection rate to 2.6 % and 2.1 % for MET-11 and MET-08 respectively. Examination of the FRP-PIXEL quality assurance (QA) information indicates that 57 % of the MET-11 observations were cloud free, 33 % were cloud obscured, 6 % were located at a cloud edge, and the remainder either sunglint affected or where the background temperature could not be estimated. Analysis of the MET-08 IODC product indicated that of the 52 burns, the FRP-PIXEL product detected one (a detection rate of 1.9 %) having an FRP of 72 MW. For the data matching EBP fires, FRP-PIXEL QA analysis indicated 63 % of the observations were cloud free, 24 % were cloud obscured, 1 % were at a cloud edge and the remainder were sunglint affected or the background temperature could not be resolved. Only including those EBP fires which are cloud free results in a detection rate to 4.9 % and 8.3 % for MET-11 and MET-08 respectively.

A cause of the high omission rate is that, whilst in theory being sufficiently large and intense enough to be detected by SEVIRI, they may not be in practice. The fires short-lived nature (average duration of 32

min) mean they are often only actively burning during a single SEVIRI imaging slot. Fig. S3a shows the FRP time-series derived from helicopter-borne MWIR imagery for a fire conducted in August 2019. The FRP remains below 15 MW much of the time, only briefly rising above 30 MW where detection by SEVIRI becomes more likely (Roberts et al., 2015). Fig. 8 shows the MET-08 and MET-11 modal per-pixel FRP value between 2017 and 2020, derived using 5 MW bins and as a function of view zenith angle $(0 - 70^{\circ})$. Over KNP, FRP retrievals from MET-11 and MET-08 are most frequently between 30—35 MW. This is higher than most of the timeseries shown Fig. S3a, and this fire occurred in August when fire intensity is typically higher than at other times of year (Govender et al., 2006). Over the KNP, SEVIRIs pixel area for MET-11 and MET-08 is 14.1 km² and 11.2 km² respectively, whilst the experimental burn plots cover a mean area of 0.067 km² (~0.47 and 0.59 % of a MET-11 and MET-08 pixel respectively). The fraction of the plot that is flaming at the time of a SEVIRI image acquisition is smaller still (10 \times lower by our estimate). Given their short duration and small size relative to the SEVIRI pixel area it is unsurprising that successful detections are infrequent.

4.4. FRP retrieval assessment

Fig. 9 presents a comparison of the FRP determined from the helicopter-borne infrared imagery and the MET-11 and MET-08 SEVIRI instruments over five fires in KNP. The mean percentage difference between the MWIR camera and satellite FRP is -11.1 and -57.3 % respectively for MET-11 and MET-08, whilst for the LWIR camera FRP -32 % (range -71 to 31 %) and -43 % (range -140 to -1.3 %) respectively for MET-11 and MET-08. Overestimation of low (\leq 40 MW) FRP fires by coarse spatial resolution sensors is also evident in comparisons between SEVIRI and MODIS (Roberts and Wooster, 2008) and GOES and MODIS (Xu et al., 2010; Schroeder et al., 2010). Table 1 shows that the FRP from the thermal camera data ranges between 14 and 66 MW, whilst the most frequently detected fires over KNP by SEVIRI are those with FRP retrievals of 30—35 MW (Fig. 8). Only one of the five EBP fires imaged simultaneously from the helicopter were successfully detected by the MET-11 and MET-08 FRP-PIXEL products (grey shaded cells in Table 1), and these had a camera measured FRP > 40 MW. The fire on the 16th October was detected by both SEVIRI instruments with the MET-11 FRP being 50 MW higher than that of MET-08 due to two AF pixels being detected in the former and only one in the latter.

Two fires in Table 1 have FRP magnitudes far below SEVIRIs detection capability, since their BT difference between the fire pixel and ambient background lies between 1-2 K. These fires are only likely to be detected by MODIS, SLSTR or VIIRS which can detect fires with an FRP between 2 and 10 MW (Li et al., 2020). Fig. 9 indicates that the airborne LWIR FRP is underestimated compared to the airborne MWIR retrievals which is also an underestimate due to the omission of fire pixels < 485 K. Vegetation fires typically have temperatures between 700—1400 K (Riggan et al., 2004) and at these temperatures the measured BT at pixels covered only partly by flame is significantly higher in the MWIR than in the LWIR (Fig. 3). Also shown in Fig. 9 is LWIR camera FRP adjusted based the relationship found between the LWIR and MWIR camera FRP (Fig. 4). The adjusted LWIR FRP reduces the average percentage difference to 21 % (-1.1 to 58.9 %) and 14 % (-43.2 to 39 %) for MET-11 and MET-08 respectively. These results though indicate that reference data for satellite FRP product evaluation should be derived from MWIR rather than LWIR imagery wherever possible.

4.5. Discussion

Satellite-derived FRP measures represent an Essential Climate Variable (ECV) and are increasingly widely used (Wooster et al., 2021), so evaluating these retrievals is important for ensuring their consistency and appropriateness for use. This study provides an overview of some of

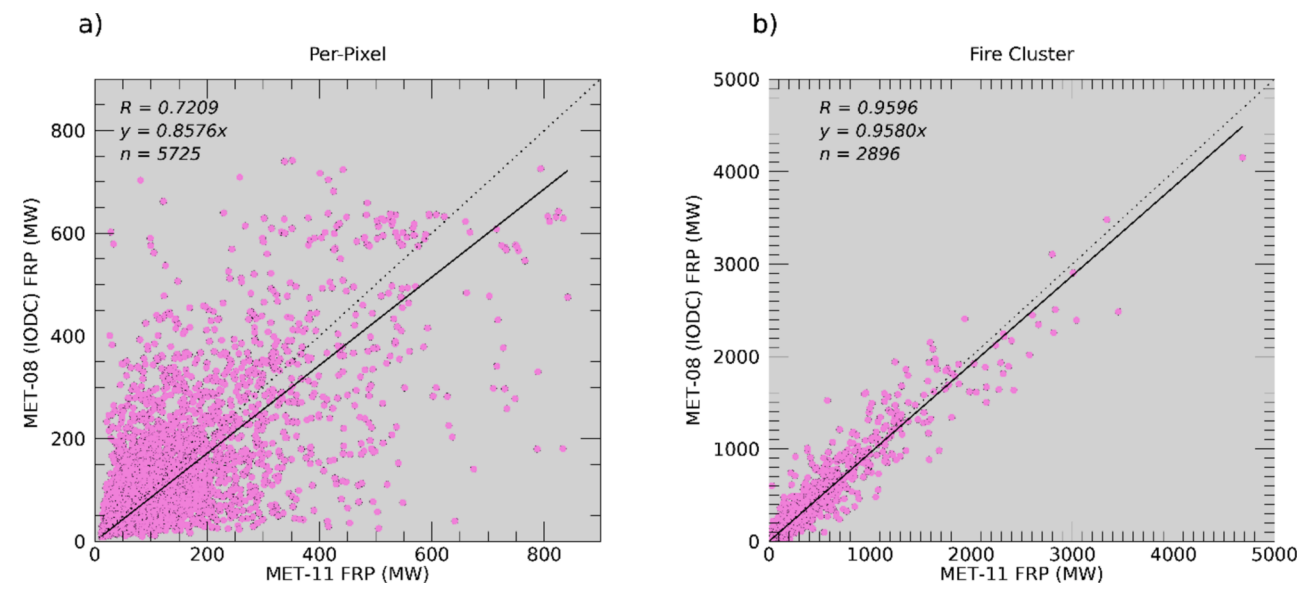


Fig. 7. Per-pixel and per-fire cluster intercomparisons of FRP retrievals obtained for the same KNP fires simultaneously from the MET-11 and MET-08 IODC over KNP between 2017 and 2020.

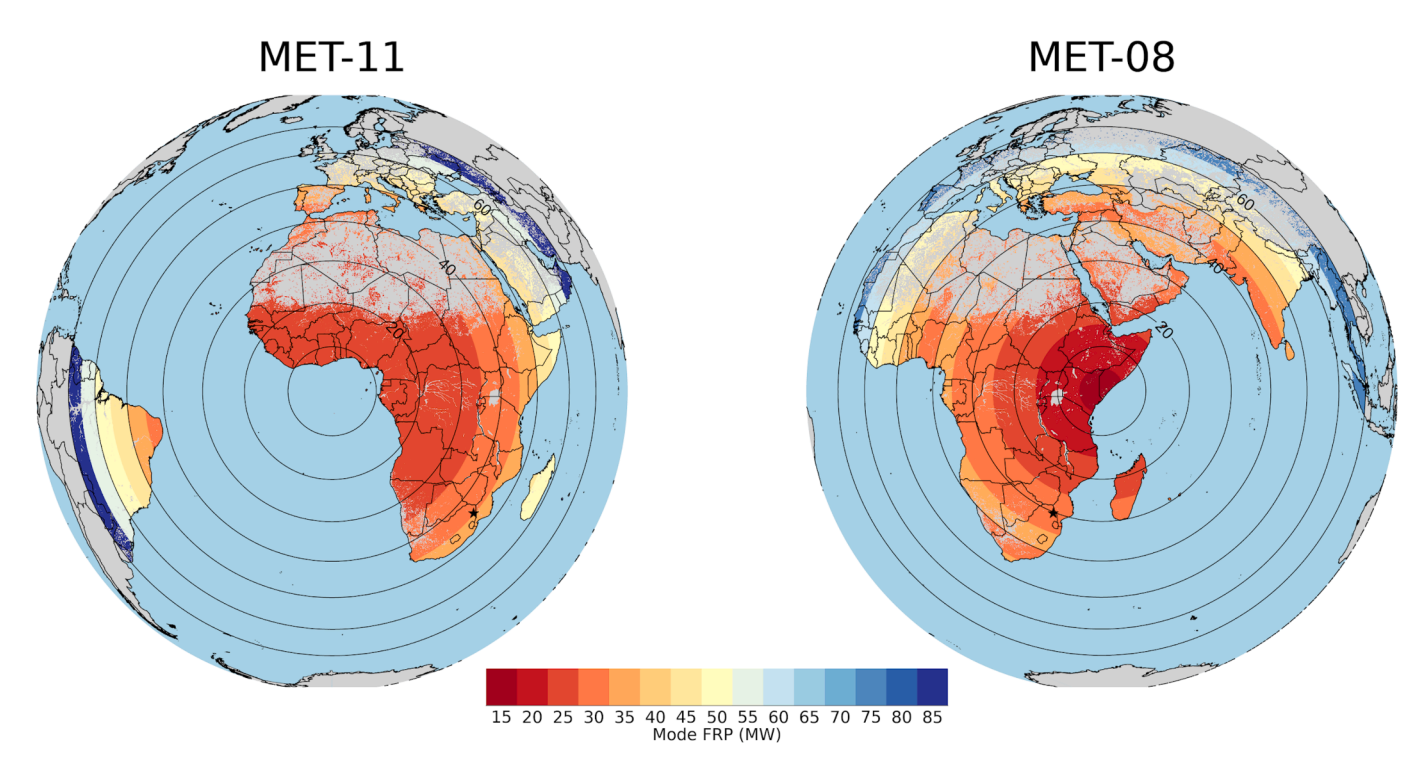


Fig. 8. Modal per-pixel FRP (MW) as a function of view zenith angle (VZA, 0-70°). All locations within a VZA band where an AF was detected contribute to the data of that band. KNP is marked by black star and data are 2017–2020.

the key factors believed to influence satellite FRP retrievals, using those from SEVIRI as an example.

At moderate and coarse spatial resolution, the location of a fire within the IFOV plays an important role in its detection, FRP retrieval, the distribution of radiance into neighbouring pixels, the number of fire pixels detected and the extent of pixel saturation. The SEVIRI imaging process was simulated to assess the influence of a fire's location within the IFOV on the retrieved FRP. At nadir, the FRP differs by up to 14 % relative to that retrieved at the pixel centre depending on the fires' location in the across-scan direction. In the case of SEVIRI, the fires' location, temperature and size influence the image FRP through the

number of detected and saturated fire pixels (Fig. 5). Schroder et al. (2010) investigated the influence of PSF weighting and fire location on FRP retrievals from MODIS and GOES which were found to decrease by ~ 66 and 50 % when the fire was located 700 and 2200 m from the pixel centre respectively. When intercomparing simulated MET-11 and -08 FRP retrievals, which have different pixel areas, the difference in fire cluster FRP can be as high as 55 % depending on the fire location, with an average median difference of 21 % (Fig. 6). The simulations conducted here greatly simplify the imaging process, as was also the case for a similar study of Sentinel-3 SLSTR (Xu et al., 2021), and a more comprehensive assessment can be found in Coppo (2015). Further

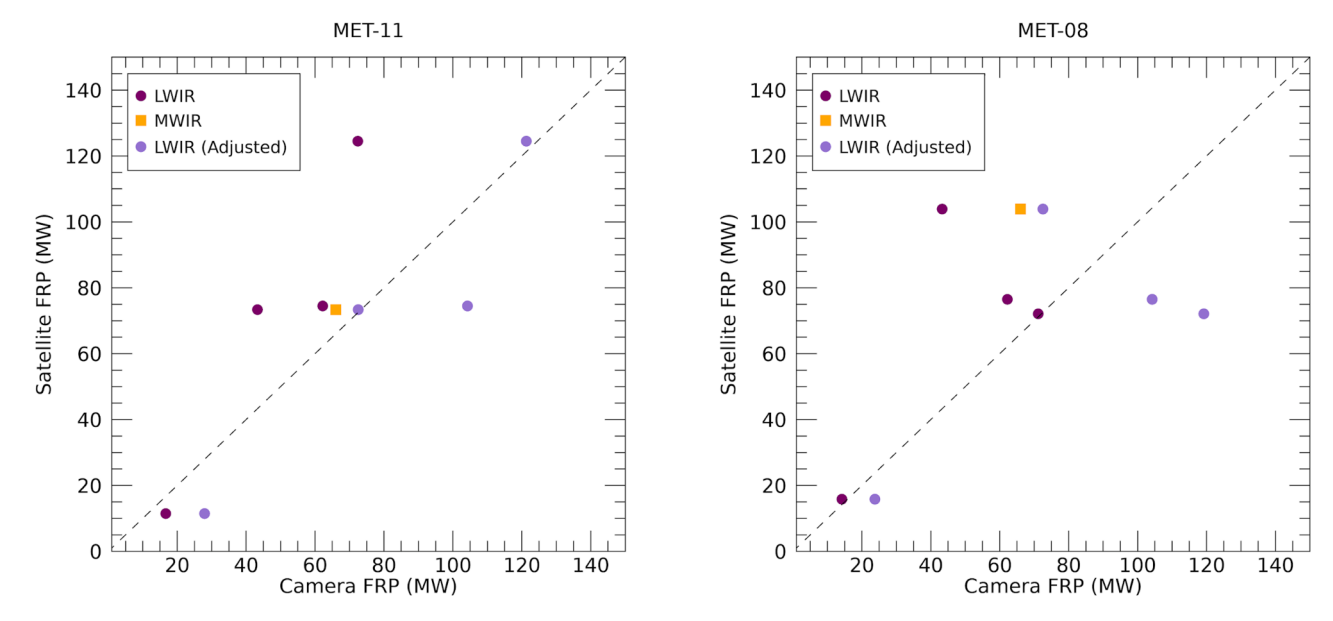


Fig. 9. FRP retrievals for five EBP fires conducted in KNP as derived from the helicopter borne MWIR and LWIR imagery and near-coincidentally from the SEVIRI instruments on MET-11 and MET-08. The 'LWIR Adjusted' data are LWIR-derived FRP adjusted using the relationship shown in Fig. 4 (to make them a closer representation of what would be derived using the MWIR).

Table 1 Temporal characteristics of the coincident SEVIRI and thermal camera FRP retrievals. Grid cells shaded grey are fires detected by the FRP-PIXEL product. Cells shaded in blue are those where the BT difference between the fire pixel and ambient background is < 1 K.

Year	Month	Day	MET-11 FRP (MW)	MET-08 FRP (MW)	AGEMA FRP (MW)	LWIR FRP (MW)	AGEMA Time Offset (seconds)	LWIR Time Offset (seconds)
2017	August	29		15.82		14.19		1
2017	August	30	11.46			16.67		20
2018	October	16	74.47	76.49		62.21		1
2018	October	16	124.5	72.1		72.40		1
2019	August	27	73.37	103.9	66.02	43.29	1	1

differences influenced by e.g. atmospheric path length differences, subpixel cloud and radiance interception by foliage could be assessed using radiative transfer models such as the Discrete Anisotropic Radiative Transfer (Gastellu-Etchegorry et al., 2015) such as that carried out by Roberts et al. (2018) to investigate the extent of fire emitted radiance interception by overlying vegetation.

Nevertheless, despite the simplicity of our simulations, the intercomparison of real MET-11 and MET-08 FRP retrievals (Fig. 7) confirms the variability seen in per-pixel FRP found in the simulations, and on a per-pixel basis we find high scatter (101.1 MW) in the almost simultaneous observations made by the two sensors from different viewing angles which is contributed to for example by differences in pixel area and thus non-fire background characterisation (Zhukov et al., 2006), sub-pixel fire location (e.g. Calle et al., 2009; Wooster et al., 2015), fire emitted radiance interception by overlying vegetation (Mathews et al., 2016; Roberts et al., 2018), and possibly atmospheric path differences (Peterson and Wang, 2013). The mean per-pixel difference (15.7 %) is close to the 26.6 % found for MODIS by Freeborn et al. (2014). When the AF pixel data are aggregated to fire pixel clusters, the degree of difference is much reduced, and we can confirm that this approach provides a more consistent method for FRP product intercomparison.

Numerous methods exit for assessing the detection rate of AF data-sets. Here, the FRP-PIXEL product detection rate was assessed using EBP fires in the KNP. The comparison was not very productive as the MET-11 and MET-08 FRP-PIXEL products detected less than 5 % and 9 % of the cloud free prescribed fires conducted in August and October between 2004 and 2018. The low detection rate is explained by SEVIRIs large pixel area over the KNP (> 11.5 km²), coupled with the small fire size (\ll

7 ha actively burning) and their low intensity (often < 20 MW, Fig. S3a). Compared to these prescribed fires, AF detections from contemporaneous Sentinel-2 (Hu et al., 2021) or Landsat data (Schroeder et al., 2008) would enable better assessment of SEVIRIs AF detection capability and as a function of the AF size and SEVIRIs pixel area (e.g. Hall et al. 2019).

We did however use some of the EBP fires to collect reference FRP data from helicopter mounted thermal imagers operating in the MWIR and LWIR spectral regions. The mean percentage difference between MET-11 and MET-08 FRP retrievals and the MWIR-derived reference data is -11.1 and $-57.3\ \%$ respectively, whilst for the LWIR is $-32\ \%$ and $-43\ \%$ respectively (decreasing to 21 % and 14 % when the LWIR measures are adjusted to better match those collected using the MWIR system). The differences we find fall within the range found both in our simulations and the MET-11 and MET-08 FRP intercomparisons. We recommend FRP reference data be collected using MWIR-based systems wherever possible, since this is the waveband used for the satellite FRP retrievals. This can be further improved by using specific bandpass filters that replicate the spectral response of the satellite waveband such as that described by Xu et al. (2021) when validating SLSTR FRP.

4.6. Conclusion

This paper presents an assessment of some of the factors that influence FRP retrieval and its validation using simulated and real SEVIRI data. SEVIRIs imaging process was found to cause differences of up to 55 % depending on the fire temperature, location within the IFOV and the viewing geometry. These results were corroborated whilst

intercomparing MET-08 and MET-11 FRP where the average per-pixel difference was 15.7 %. The active fire detection rate of SEVIRI was found to be between 5 and 9 % when assessed against EBP fires that occurred in August and October when fires are their most intense. The low detection rate is explained by SEVIRIs large pixel area over the region (> 11 km²), the small fire size (average size < 7 ha) and their low FRP (typically < 30 MW). Helicopter mounted thermal camera imagery were used to validate SEVIRI FRP which revealed SEVIRI tended to overestimate FRP depending on the Meteosat platform used and the spectral wavelength of the camera imagery. Our results indicate the factors assessed here should be taken into consideration when defining uncertainty thresholds for GCOS requirements and in developing satellite FRP product validation protocols. Currently, FRP is at CEOS validation stage one and, despite the challenges in validating FRP retrievals, it is important to build on this. To do so, support from space agencies is needed for validation campaigns to ensure the long-term consistency of active fire and FRP products.

CRediT authorship contribution statement

Gareth Roberts: Writing – review & editing, Writing – original draft, Visualization, Methodology, Funding acquisition, Conceptualization. Martin. J. Wooster: Writing – review & editing, Methodology, Funding acquisition. Tercia Strydom: Resources, Data curation.

Declaration of competing interest

The authors declare that they have no known competing financial interests or personal relationships that could have appeared to influence the work reported in this paper.

Acknowledgments

We would like to thank South African National Parks (SANParks), the KNP Scientific Services (grant WOOM1421), the KNP Fire Team, Navashni Govender and Jacques (pilot) for their support in conducting this research. We would like to thank the LSA-SAF, EUMETSAT and Copernicus for provision of the data. We would like to thank the reviewers for their comments in improving the manuscript. Funding for this research was provided by NERC grants (NE/M017958/1; NE/M017729/1) and M Wooster was also supported by the National Centre for Earth Observation (NCEO, NE/R016518/1).

Appendix A. Supplementary data

Supplementary data to this article can be found online at https://doi.org/10.1016/j.jag.2025.104375.

Data availability

Data will be made available on request.

References

- Biggs, R., Biggs, H.C., Dunne, T.T., Govender, N., Potgieter, A.L.F., 2003. Experimental burn plot trial in the Kruger National Park: history, experimental design and suggestions for data analysis. *Koedoe* 46 (1), 1–15.
- Boschetti, L., Roy, D.P., Giglio, L., Huang, H., Zubkova, M., Humber, M.L., 2019. Global validation of the collection 6 MODIS burned area product. *Rem. Sens. Environ* 235, 111490.
- Calle, A., Casanova, J.L., Gonzalez-Alonso, F., 2009. Impact of point spread function of MSG-SEVIRI on active fire detection. *Int. J. Rem. Sens* 30 (17), 4567–4579.
- Coppo, P., 2015. Simulation of fire detection by infrared imagers from geostationary satellites. Rem. Sens. Environ 162, 84–98.
- Dickinson, M.B., Hudak, A.T., Zajkowski, T., Loudermilk, E.L., Schroeder, W., Ellison, L., Kremens, R.L., Holley, W., Martinez, O., Paxton, A., Bright, B.C., 2016. Measuring radiant emissions from entire prescribed fires with ground, airborne and satellite sensors–RxCADRE 2012. Int. J. Wildland Fire 25 (1), 48–61.

- Freeborn, P.H., Wooster, M.J., Roberts, G., 2011. Addressing the spatiotemporal sampling design of MODIS to provide estimates of the fire radiative energy emitted from Africa. Remote Sens. Environ. 115 (2), 475–489.
- Freeborn, P.H., Wooster, M.J., Roy, D.P., Cochrane, M.A., 2014. Quantification of MODIS fire radiative power (FRP) measurement uncertainty for use in satellite-based active fire characterization and biomass burning estimation. *Geophys. Res. Letters* 41 (6), 1988, 1904
- Gastellu-Etchegorry, J.P., Yin, T., Lauret, N., Cajgfinger, T., Gregoire, T., Grau, E., Feret, J.B., Lopes, M., Guilleux, J., Dedieu, G., Malenovský, Z., 2015. Discrete anisotropic radiative transfer (DART 5) for modeling airborne and satellite spectroradiometer and LIDAR acquisitions of natural and urban landscapes. Remote Sens. 7 (2), 1667–1701.
- Giglio, L., Csiszar, I., Justice, C.O., 2006. Global distribution and seasonality of active fires as observed with the Terra and Aqua Moderate Resolution Imaging Spectroradiometer (MODIS) sensors. J. Geophys. Res. Biogeosciences 111 (G2).
- Giglio, L., Schroeder, W., Justice, C.O., 2016. The collection 6 MODIS active fire detection algorithm and fire products. Rem. Sens. Environ 178, 31–41.
- Govender, N., Trollope, W.S., Van Wilgen, B.W., 2006. The effect of fire season, fire frequency, rainfall and management on fire intensity in savanna vegetation in South Africa. J. Appl. Ecol 43 (4), 748–758.
- Hall, J.V., Zhang, R., Schroeder, W., Huang, C., Giglio, L., 2019. Validation of GOES-16 ABI and MSG SEVIRI active fire products. Int. J. Appl. Earth Obs. Geoinf 83, 101928.
- Hu, X., Ban, Y., Nascetti, A., 2021. Sentinel-2 MSI data for active fire detection in major fire-prone biomes: A multi-criteria approach. *Int. J. Appl. Earth Obs. Geoinf* 101, 102347
- Jin, Y., Randerson, J.T., Goetz, S.J., Beck, P.S., Loranty, M.M., Goulden, M.L., 2012. The influence of burn severity on postfire vegetation recovery and albedo change during early succession in North American boreal forests. *J. Geophys. Res. Biogeosciences* 117 (G1).
- Kumar, S.S., Hult, J., Picotte, J., Peterson, B., 2020. Potential Underestimation of Satellite Fire Radiative Power Retrievals over Gas Flares and Wildland Fires. Rem. Sens 12 (2), 238.
- Li, F., Zhang, X., Kondragunta, S., Csiszar, I., 2018. Comparison of fire radiative power estimates from VIIRS and MODIS observations. J. Geophys. Res. Atmospheres 123 (9), 4545–4563.
- Li, F., Zhang, X., Kondragunta, S., Schmidt, C.C., Holmes, C.D., 2020. A preliminary evaluation of GOES-16 active fire product using Landsat-8 and VIIRS active fire data, and ground-based prescribed fire records. *Rem. Sens. Environ* 237, 111600.
- Lizundia-Loiola, J., Otón, G., Ramo, R., Chuvieco, E., 2020. A spatio-temporal active-fire clustering approach for global burned area mapping at 250 m from MODIS data. *Rem. Sens. Environ* 236, 111493.
- Mathews, B.J., Strand, E.K., Smith, A.M., Hudak, A.T., Dickinson, B., Kremens, R.L., 2016. Laboratory experiments to estimate interception of infrared radiation by tree canopies. Int. J. Wildland Fire 25 (9), 1009–1014.
- Morisette, J.T., Baret, F., Privette, J.L., Myneni, R.B., Nickeson, J.E., Garrigues, S., Shabanov, N.V., Weiss, M., Fernandes, R.A., Leblanc, S.G., Kalacska, M., 2006. Validation of global moderate-resolution LAI products: A framework proposed within the CEOS land product validation subgroup. *IEEE Trans. Geosci. Remote Sens* 44 (7), 1804–1817.
- Paugam, R., Wooster, M.J., Roberts, G., 2012. Use of handheld thermal imager data for airborne mapping of fire radiative power and energy and flame front rate of spread. *IEEE Trans. Geosci. Remote Sens* 51 (6), 3385–3399.
- Paugam, R., Wooster, M.J., Mell, W.E., Rochoux, M.C., Filippi, J.B., Rücker, G., Frauenberger, O., Lorenz, E., Schroeder, W., Main, B., Govender, N., 2021. Orthorectification of helicopter-borne high resolution experimental burn observation from infra-red handheld imagers. Remote Sens. 13 (23), 4913.
- Peterson, D., Wang, J., 2013. A sub-pixel-based calculation of fire radiative power from MODIS observations: 2. Sensitivity analysis and potential fire weather application. *Rem. Sens. Environ* 129, 231–249.
- Riggan, P.J., Tissell, R.G., Lockwood, R.N., Brass, J.A., Pereira, J.A.R., Miranda, H.S., Miranda, A.C., Campos, T., Higgins, R., 2004. Remote measurement of energy and carbon flux from wildfires in Brazil. *Ecological Applications* 14 (3), 855–872.
- Roberts, G.J., Wooster, M.J., 2008. Fire detection and fire characterization over Africa using Meteosat SEVIRI. *IEEE Trans. Geosci. Remote Sens* 46, 1200–1218.
- Roberts, G., Wooster, M.J., Lagoudakis, E., 2009. Annual and diurnal African biomass burning temporal dynamics. *Biogeosciences* 6 (5), 849–866.
- Roberts, G., Wooster, M.J., Xu, W., Freeborn, P.H., Morcrette, J.J., Jones, L., Benedetti, A., Jiangping, H., Fisher, D., Kaiser, J.W., 2015. LSA SAF Meteosat FRP products–Part 2: Evaluation and demonstration for use in the Copernicus Atmosphere Monitoring Service (CAMS). Atmos. Chem. Phys 15 (22), 13241–13267.
- Roberts, G., Wooster, M.J., Lauret, N., Gastellu-Etchegorry, J.P., Lynham, T., McRae, D., 2018. Investigating the impact of overlying vegetation canopy structures on fire radiative power (FRP) retrieval through simulation and measurement. Rem. Sens. Environ 217, 158–171.
- Roberts, G., Wooster, M.J., 2021. Global impact of landscape fire emissions on surface level PM2. 5 concentrations, air quality exposure and population mortality. Atmos. Environ., 118210
- Schmetz, J., Pili, P., Tjemkes, S., Just, D., Kerkmann, J., Rota, S., Ratier, A., 2002. An introduction to Meteosat second generation (MSG). B. Am. Meteorol. Soc 83 (7), 977–992
- Schmidt, C.C., Hoffman, J., Prins, E., Lindstrom, S., 2012. GOES-R Advanced Baseline Imager (ABI) Algorithm Theoretical Basis Document for Fire/Hot Spot Characterization, Version 2.5, edited, pp. 1–97, NOAA NESDIS STAR.
- Schroeder, W., Prins, E., Giglio, L., Csiszar, I., Schmidt, C., Morisette, J., Morton, D., 2008. Validation of GOES and MODIS active fire detection products using ASTER and ETM+ data. *Rem. Sens. Environ* 112 (5), 2711–2726.

- Schroeder, W., Csiszar, I., Giglio, L., Schmidt, C.C., 2010. On the use of fire radiative power, area, and temperature estimates to characterize biomass burning via moderate to coarse spatial resolution remote sensing data in the Brazilian Amazon. J. Geophys. Res. Atmospheres 115 (D21).
- Schroeder, W., Oliva, P., Giglio, L., Csiszar, I.A., 2014a. The New VIIRS 375 m active fire detection data product: Algorithm description and initial assessment. *Rem. Sens. Environ* 143, 85–96.
- Schroeder, W., Ellicott, E., Ichoku, C., Ellison, L., Dickinson, M.B., Ottmar, R.D., Clements, C., Hall, D., Ambrosia, V., Kremens, R., 2014b. Integrated active fire retrievals and biomass burning emissions using complementary near-coincident ground, airborne and spaceborne sensor data. *Rem. Sens. Environ* 140, 719–730.
- Trigo, I.F., Dacamara, C.C., Viterbo, P., Roujean, J.L., Olesen, F., Barroso, C., Camacho-de-Coca, F., Carrer, D., Freitas, S.C., García-Haro, J., Geiger, B., 2011. The satellite application facility for land surface analysis. *Int. J. Rem. Sens* 32 (10), 2725–2744.
- van der Werf, G.R., Randerson, J.T., Giglio, L., Leeuwen, T.T.V., Chen, Y., Rogers, B.M., Mu, M., Van Marle, M.J., Morton, D.C., Collatz, G.J., Yokelson, R.J., 2017. Global fire emissions estimates during 1997–2016. *Earth Syst. Sci. Data* 9 (2), 697–720.
- Vermote, E., Ellicott, E., Dubovik, O., Lapyonok, T., Chin, M., Giglio, L., Roberts, G.J., 2009. An approach to estimate global biomass burning emissions of organic and black carbon from MODIS fire radiative power. J. Geophys. Res. Atmospheres 114 (D18).
- Wickramasinghe, C., Wallace, L., Reinke, K., Jones, S., 2018. Intercomparison of Himawari-8 AHI-FSA with MODIS and VIIRS active fire products. Int. J. Digit. Earth 13 (4), 457–473.
- Wooster, M.J., Xu, W., Nightingale, T., 2012. Sentinel-3 SLSTR active fire detection and FRP product: Pre-launch algorithm development and performance evaluation using MODIS and ASTER datasets. Rem. Sens. Environ 120, 236–254.

- Wooster, M.J., Roberts, G., Freeborn, P.H., Xu, W., Govaerts, Y., Beeby, R., He, J., Lattanzio, A., Mullen, R., 2015. Meteosat SEVIRI Fire Radiative Power (FRP) products from the Land Surface Analysis Satellite Applications Facility (LSA SAF) –Part 1: Algorithms, product contents and analysis. Atmos. Chem. Phys 15 (15), 13217–13239.
- Wooster, M.J., Roberts, G.J., Giglio, L., Roy, D.P., Freeborn, P.H., Boschetti, L., Justice, C., Ichoku, C., Schroeder, W., Davies, D., Smith, A.M., 2021. Satellite remote sensing of active fires: History and current status, applications and future requirements. *Rem. Sens. Environ.* 267, 112694.
- Xu, W., Wooster, M.J., Roberts, G., Freeborn, P., 2010. New GOES imager algorithms for cloud and active fire detection and fire radiative power assessment across North, South and Central America. Rem. Sens. Environ 114 (9), 1876–1895.
- Xu, W., Wooster, M.J., Kaneko, T., He, J., Zhang, T., Fisher, D., 2017. Major advances in geostationary fire radiative power (FRP) retrieval over Asia and Australia stemming from use of Himarawi-8 AHI. Rem. Sens. Environ 193, 138–149.
- Xu, W., Wooster, M.J., Polehampton, E., Yemelyanova, R., Zhang, T., 2021. Sentinel-3 active fire detection and FRP product performance-Impact of scan angle and SLSTR middle infrared channel selection. Rem. Sens. Environ 261, 112460.
- Xue, T., Geng, G., Li, J., Han, Y., Guo, Q., Kelly, F.J., Wooster, M.J., Wang, H., Jiangtulu, B., Duan, X., Wang, B., 2021. Associations between exposure to landscape fire smoke and child mortality in low-income and middle-income countries: a matched case-control study. *Lancet Planet Health* 5 (9), e588–e598.
- Zhukov, B., Lorenz, E., Oertel, D., Wooster, M., Roberts, G., 2006. Spaceborne detection and characterization of fires during the bi-spectral infrared detection (BIRD) experimental small satellite mission (2001–2004). Rem. Sens. Environ 100 (1), 29–51.